JPL PUBLICATION 84-70

(NASA-CR-174260) TARGET DETECTION USING MICROWAVE IRRADIANCES FROM NATURAL SOURCES: A PASSIVE, LOCAL AND GLOBAL SURVEILLANCE SYSTEM (Jet Propulsion Lab.) 38 p HC A03/MF A01 CSCL 09C G3/33

N85-15991

Unclas 13395

Target Detection Using Microwave Irradiances From Natural Sources

A Passive, Local and Global Surveillance System

J.M. Stacey

November 15, 1984

National Aeronautics and Space Administration

Jet Propulsion Laboratory
California Institute of Technology
Pasadena, California

JPL PUBLICATION 84-70

Target Detection Using Microwave Irradiances From Natural Sources

A Passive, Local and Global Surveillance System

J.M. Stacey

November 15, 1984

NASA

National Aeronautics and
Space Administration

Jet Propulsion Laboratory
California Institute of Technology
Pasadena, California

The research described in this publication was carried out by the Jet Propulsion Laboratory, California Institute of Technology, under a contract with the National Aeronautics and Space Administration.

TABLE OF CONTENTS

ABSTRACT

This report describes the results of an investigation to detect metal objects on or near the Earth's surface using existing, passive, microwave sensors operating from Earth orbit.

The range equations are derived from basic microwave principles and theories and the expressions are given explicitly to estimate the signal-to-noise ratio for detecting metal targets operating as bistatic scatterers.

Actual measurements are made on a range of metal objects observed from orbit using existing passive microwave receiving systems. The details of the measurements and the results are tabulated and discussed.

The investigation is mainly focussed to show the advantages of a passive microwave sensor as it is applied to surveillance of metal objects as viewed from aerial platforms or from orbit.

DISCUSSION

Described here is a verified concept for detecting point targets such as aircraft, ships, buoys, etc., from an airborne or orbiting vehicle by using a passive, microwave, sensor system and by using the irradiances from natural phenomena as the source of the illumination for the target. The natural phenomena that serve as sources of the illumination are identified as the gaseous and particulate matter in the troposphere and the cosmic background blackbody radiation.

Where an airborne or orbiting vehicle views a point target or a reflective earth area at a lower altitude, the reflective properties of the target produce a thermodynamic difference temperature between the target and the projected earth background as viewed by the antenna system. It is this difference temperature that serves as a point source of illumination which operates to identify the occurrence and location of the target.

Where the Earth's atmosphere and the cosmic background radiation are reflected from a metallic target with the sea or terrain serving as the background temperature, the highly reflective properties of the target produce a cold signature with respect to the background. It is this cold signature which uniquely identifies the occurrence and location of the target as projected against the geodetic coordinates of the Earth. The microwave radiance P_i that is reflected by the target into the antenna system of the airborne or orbiting system is given by

$$P_i = k\,(T_B - T_{CA}),\ \text{watts/hertz} \qquad (1)$$

where

k = Boltzmann constant

T_B = Earth-background temperature, K

T_C = Cosmic-background temperature, 2.7 K, a true blackbody radiation, K

T_A = Thermodynamic temperature of the atmospheric constituents, K

T_{CA} = Combined thermodynamic temperature given by T_C and T_A, K

P_i may be considered to be a point source of radiance because, in the practical sense, the angle subtended by the target from the antenna system is small compared with the angle subtended by its background. P_i is directly proportional to the difference between the reflected target temperature and its mean background temperature.

Fig. 1 illustrates the geometry of the concept as it applies to the target detection method described here. The target is shown as a metallic object, an aircraft with a high reflectivity factor and with a complementary low emissivity factor.

Crucial to the success of the concept is that the natural sources of illumination are distributed over 2π steradians (hemispherical coverage) within the view of the target and the antenna system. Because of the hemispherical coverage of the natural sources of the irradiance in the downwelling path incident on the target, there will always occur a complementary forward scatter angle and directivity pattern in the direction of the antenna system.

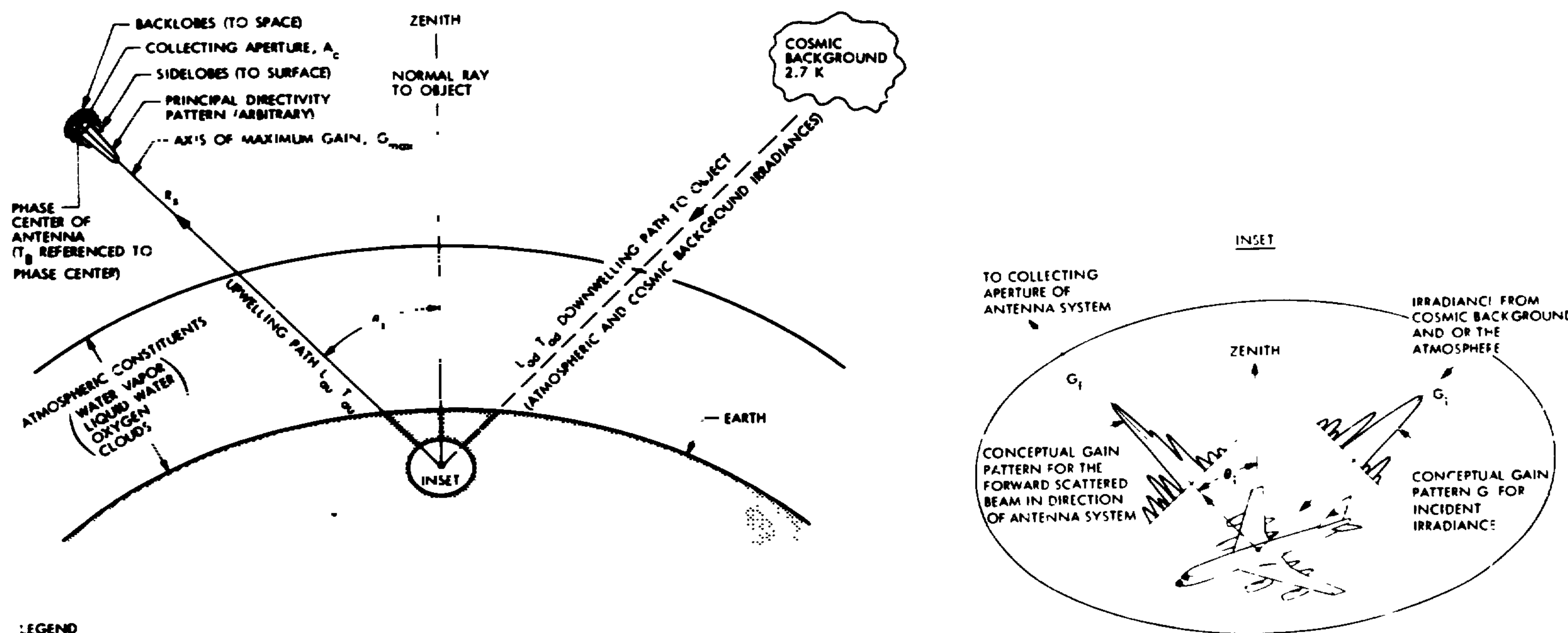

LEGEND

T_{ou} = INTEGRATED PHYSICAL TEMPERATURE OF THE UPWELLING PATH, K

L_{ou} = LOSS IN THE UPWELLING PATH

T_{surf} = PHYSICAL TEMPERATURE OF THE SURFACE MATERIAL, K

L_{surf} = LOSS IN THE SURFACE MATERIAL

T_{od} = INTEGRATED PHYSICAL TEMPERATURE OF THE DOWNWELLING PATH, K

L_{od} = LOSS DOWNWELLING PATH, K

T_B = THERMODYNAMIC TEMPERATURE OF THE BACKGROUND, K

R_s = SLANT RANGE (COLLECTING APERTURE TO OBJECT), m

A_c = AREA OF COLLECTING APERTURE, m^2

G_{max} = AXIS OF MAXIMUM ANTENNA GAIN

θ_i = INCIDENCE ANGLE, deg

$$T_B = \underbrace{\frac{T_{cosmic}}{L_{od}\,L_{surf}\,L_{ou}}}_{[\text{COSMIC}]} + \underbrace{\frac{T_{od}\,(L_{od}-1)}{L_{od}\,L_{surf}\,L_{ou}}}_{[\text{DOWNWELLING}]} + \underbrace{\frac{T_{surf}\,(L_{surf}-1)}{L_{surf}\,L_{ou}}}_{[\text{SURFACE}]} + \underbrace{\frac{T_{ou}\,(L_{ou}-1)}{L_{ou}}}_{[\text{UPWELLING}]},\ K$$

WHERE: E = EMISSIVITY

$$L_{surf} = \frac{1}{1-E}$$

SUBSCRIPTED L SYMBOLS ARE DISSIPATIVE LOSSES EXPRESSED AS A NUMBER > 1.

Fig. 1. Thermodynamic transfer of temperature

Particular structural members of the target will always be oriented or disposed to operate as a collecting area A_i with receiving gain G_i in the direction of the incident irradiance. From this irradiance the target operates as an electrically excited structure with area A_f and with gain G_f in the forward scattered direction of the antenna system along the upwelling path. The incident radiation vector along the downwelling path and the axis of the forward scattered gain pattern of the target form complementary angles about the zenith which are approximately equal to the angle of incidence θ_i. Because of the hemispherical distribution of the irradiance of the natural sources this geometrical relationship will always be true. Further, the antenna system will view the target as a temperature gradient (usually a cold point) projected against the earth background T_B. From this P_i (1) is conceived as a point source of illumination whose magnitude is proportional to the difference between the earth background and the combined temperatures of the natural sources T_{CA} when the target is immersed in the atmosphere and from the cosmic background temperature T_C when the target is above the atmosphere. Apparently, high altitude aircraft will produce stronger radiances as observed by an earth-orbiting antenna system than aircraft operating near the surface.

The geometry and the concept are depicted in Fig. 1. The terms of the expression for the transfer of thermodynamic temperatures from the cosmic background to the collecting aperture of the antenna system are shown as they relate to the downwelling path, inset area on the Earth, and the upwelling path. T_B is the apparent background temperature observed by the antenna system at any instant in time.

From the model and the geometry shown in Fig. 1 and with the consideration that P_i serves as a point source of illumination that is reradiated from the metal target and scattered in the forward direction into the collecting area A_c of the antenna system:

$$P_r = P_i \; G_i \; G_f \frac{1}{4\pi \; R_s^{\,2}} A_c, \text{ watts/hertz} \tag{2}$$

by substitution in (1), and with the preliminary simplification that $G_i = G_f$ and that $G_i \; G_f = G_T^{\,2}$,

R_s = Slant range between target and antenna system in meters.

P_r = Power available at the antenna terminals.

Further, the collecting area of the antenna A_c is modified by the <u>solid angle beam efficiency</u> ε_{sa}.

Then

$$P_r = k \; (T_B - T_{CA}) \; G_T^{\,2} \frac{1}{4\pi \; R_s^{\,2}} \; (A_c \varepsilon_{sa}), \text{ watts/hertz} \tag{3}$$

The noise power of the receiver that is associated with the antenna system is given by

$$P_n = kT_R, \text{ watts/hertz} \tag{4}$$

where

T_R = Temperature resolution (RMS noise) of the receiver.

When the clutter noise that enters the sidelobes and backlobes of the antenna pattern through 4π steradians is combined with the RMS noise of the receiver, and both are expressed as temperatures in kelvins, then

$$P_n = k[T_{clut}^2 + T_R^2]^{1/2}, \text{ watts/hertz} \tag{5}$$

The signal-to-noise ratio is defined by

$$\frac{S}{N} = \frac{P_r}{P_n}$$

Combining (3) with (5),

$$\frac{S}{N} = \frac{k\ (T_B - T_{CA})\ G_T^2\ (A_c \varepsilon_{sa})}{4\pi R_s^2\ k[T_{clut}^2 + T_R^2]^{1/2}}, \text{ dimensionless} \tag{6}$$

Now (6) can be rewritten in more perspicuous form to facilitate numerical entries for some of the terms. By substitution in (6)

$$G_T^2 = \left(\frac{4\ \pi\ A_T}{\lambda^2}\right)^2 \tag{7}$$

where $A_i = A_f = A_T$ which are defined as the collecting areas of the target for the incident A_i and forward scatter A_f areas.

By substitution of (7) in (6)

$$\frac{S}{N} = \frac{4\pi\ (T_B - T_{CA})\ A_T^2 (A_c \varepsilon_{sa})}{R_s^2 \lambda^4 (T_{clut}^2 + T_R^2)^{1/2}}, \text{ dimensionless} \tag{8}$$

A target reflectivity factor is defined Z_r which expresses the fraction of the area of the target structure that participates in collecting the incident radiation from the natural sources and again operates to rescatter the radiation in the direction of the antenna system.

Entering Z_r in (8) and rewriting

$$\frac{S}{N} = \frac{4\pi(T_B - T_{CA})(A_T Z_R)^2(A_c \varepsilon_{sa})}{R_s^2 \lambda^4 (T_{clut}^2 + T_R^2)^{1/2} L_{au}} \text{, dimensionless} \qquad (9)$$

L_{au} is entered in (9) to account for attenuation (at wavelength λ) arising in the upwelling path.

The term $T_B - T_{CA}$ should be understood to be an absolute value. There is a class of targets (e.g., plumes and ships with wooden decks) that may possess radiances that are greater than the background T_B.

The range of the variables in (9) deserves some discussion: the range of the target background temperature T_B varies from less than 100 K for a smooth cold sea to over 300 K for a tropical forested area.

T_C as defined in (1) is the cosmic-background temperature 2.7 K $\pm$ 0.15 K (1σ) and is an appropriate entry when the target is observed above the atmosphere. When the target is operating near sea level for example the natural source irradiance from the atmosphere (water vapor, oxygen, and clouds) is a function of the operating wavelength of the antenna system. At an operating wavelength of 8 millimeters, and when the downwelling path is unaffected by raining clouds, the thermodynamic temperature of the atmosphere

T_{CA} (in combination with the cosmic background temperature) is estimated at 27 K. Users of (9) are burdened to estimate the temperature of the downwelling path and L_{au} when changes in operating wavelength occur.

The collecting areas of targets such as buoys or aircraft, are typically several hundred meters. In certain studies that investigate the relative backscattering and forward scattering properties of these targets it commonly appears that about 6% of the area is effective. Naturally this is a target peculiar situation and the user is again burdened to estimate a value for Z_r or to substitute actual measured values.

The collecting area efficiency of the antenna system is expressed by ε_{sa} where it is defined as the solid angle main beam efficiency. ε_{sa} ranges from about 60% for poor antennas with considerable blockage and multiple reflecting surfaces, to over 95% for excellent antenna designs. Antennas with offset feeds using prime-focus optics with no physical blockage of the primaries will yield ε_{sa} in excess of 95%. Solid angle beam efficiency should not be confused with the term antenna efficiency which is typically used to modify the collecting area of an antenna as used in communications and radar practice. Here again the user is burdened to understand the difference.

The RMS noise level of the antenna system receiver is expressed in kelvins. The RMS noise level is defined as the temperature resolution of the receiver. It is sometimes called "Delta Tee."

The magnitude of the clutter enterir the antenna system antenna pattern is expressed by T_{clut} in kelvin.. The temperature range of T_{clut} has been observed here for a wide range of conditions which involve orbital observations in the vicinity of ice/water, sea/land, and desert/forest boundary areas. Based on a considerable amount of experience with only a few operational antenna systems, the observed range for T_{clut} varies from less than 1 K to over 7 K. By expectation T_{clut} will exceed T_R especially for antenna systems with low values of ε_{sa}.

Observations of spacecraf (in a lower orbit), aircraft, ships, and large Discus-type buoys, taken by operational antenna systems borne on existing spacecraft, have returned a range of signal-to-noise ratios from 2 to 18 dB and are in acceptable agreement with estimated entries for the terms of (9). For these actual observations the following typical geometrical and antenna system specifications are given for the terms of (9):

T_B = 290 K

T_{CA} = 27 K

A_T : A range from 9 to 290 m^2

Z_r : Typically 0.06 (-12 dB)

A_c = 0.49 m^2

ε_{sa} = 0.90

R_S = 1122 km (maintained constant by a scanning antenna system at constant incidence angle θ_i)

λ = 0.008 m

T_{clut} : Typically 1 to 5 K

T_R = 1.5 K (reduces further by in-scan averaging)

$L_{au}(\lambda)$ = 0.35 dB = 1.08 (at 8-mm wavelength)

Figure 2 is included to summarize the application of the terms of (9).

Large Discus-type buoys (10- and 12-meter diameters) serve as excellent permanent test targets because they are moored and their locations are precisely known. Also, they are symmetrical geometrical figures and possess similar directivity patterns for G_i and G_f at the same angle of incidence θ_i. Discus buoys are abundantly distributed and return positive signal-to-noise ratios for antenna systems operating in low earth orbit.

An antenna system which operates as an autonomous sensor and is carried by an airborne vehicle or earth-orbiting spacecraft features the following:

- Emits no manmade radiation during the surveillance and therefore executes its mission undetected.

- Maintains a high invulnerability to jamming.

- The antenna system executes target detection capability with modest and practical sizes for the collecting aperture even from earth orbit.

- Surveillance can be conducted with a wide-scan capability, as a microwave imager operating in a search mode, or in a point, acquire, and track mode.

- The surveillance mission, at microwave wavelengths, is relatively invulnerable to weather. Raining clouds that fill the downwelling path are a worst case occurrence for the performance of the antenna system...an occurrence with less than a 1% probability for space-borne antenna systems.

- The antenna system sometimes uses the irradiance of the atmosphere to execute the surveillance, but is not limited by it.

- Passive antenna systems, by comparison with active systems, are smaller, lighter, and of considerably lower cost, especially for operation at large slant ranges.

$$\frac{S}{N} = \frac{4\pi(T_B - T_{CA})(A_T Z_r)^2 (A_c \epsilon_{sa})}{R_s^2 \lambda^4 (T_{clut}^2 + T_R^2)^{1/2} L_{au}} \text{, DIMENSIONLESS}$$

WHERE:

T_B = BACKGROUND TEMPERATURE FOR TARGET, K
(<100 K FOR SMOOTH COLD SEAS TO > 300 K FOR TROPICAL FORESTS.)

T_{CA} = EMISSION TEMPERATURE OF THE DOWNWELLING PATH AT THE SURFACE, K
(TYPICALLY 27 K, AT SEA LEVEL, AT MID-LATITUDES, CLEAR DAY, 8-mm WAVELENGH)

A_T = PROJECTED AREA OF TARGET AS VIEWED FROM THE ANTENNA SYSTEM, M^2
(LARGE BUOYS AND AIRCRAFT TYPICALLY RANGE FROM 100 OVER 300 M^2)

Z_r = REFLECTIVITY FACTOR FOR THE TARGET AREA, DIMENSIONLESS
(MEASURED VALUES FOR CERTAIN COMMON AIRCRAFT ARE TYPICALLY 0.06)

A_c = AREA OF THE COLLECTING APERTURE OF THE ANTENNA SYSTEM, M^2)

R_s = SLANT RANGE, TARGET TO ANTENNA SYSTEM, M

ϵ_{sa} = SOLID ANGLE MAIN BEAM EFFICIENCY OF THE ANTENNA, DIMENSIONLESS
(0.6 TO > 0.95 FOR POOR AND EXCELLENT ANTENNA DESIGNS, RESPECTIVELY)

λ = OPERATING WAVELENGTH OF THE ANTENNA SYSTEM, M

T_{clut} = RMS VALUE OF THE CLUTTER COMPONENTS ENTERING THE SIDELOBES AND BACKLOBES OF THE ANTENNA SYSTEM AND FROM THE BACKGROUND, K
(TYPICAL RANGE: 1 TO 5 K, AS DEDUCED BY ACTUAL EXPERIENCE)

T_R = RMS NOISE LEVEL OF THE ANTENNA SYSTEM RECEIVER, K
(TYPICALLY RANGES FROM 0.5 TO 1.5 K)

L_{au} = ATTENUATION IN THE UPWELLING PATH, DIMENSIONLESS
(A NUMBER > 1, TYPICALLY 1.08 [0.35 dB], AT 8-mm WAVELEN,GTH, CLEAR DAY, MID-LATITUDES.)

Fig. 2. Target detection by using the irradiances of natural sources...a passive surveillance system

APPENDIX A

OBJECTS DETECTED FROM EARTH ORBIT

Objects detected from earth orbit with positive S/N ratios that range from 2 to 18 dB: S/N predictions are given by equation (9) and are in satisfactory agreement with measured results at 8-mm wavelength.

APPENDIX B

VERIFICATIONS OF METALLIC OBJECT DETECTIONS BY SURFACE TRUTH

Current data from existing microwave receiving systems, or the archived data from previous systems, can be applied to the detection and investigation of metallic objects on or near the surface of the Earth. For this purpose, the terms of equation (9) may be adapted to estimate the expected S/N for a range of metallic objects such as aircraft, ships, and large buoys.

Where (9) is applied as an estimator for S/N, it is required that certain features of the particular object be determined such as the physical size of the reflecting area and also the character of the geometrical figure. The geometrical figure consideration is of critical importance because the reflectivity factor Z_r in (9) can assume a wide range of values depending on whether the object consists of a collection of scattering centers (e.g. an aircraft structure) or exists as a symmetrical figure such as a Discus-type buoy.

At the outset, one chooses to observe a particular class of metal objects whose physical characteristics are well defined and whose electrical properties (e.g. bistatic antenna gain patterns) can be suitably estimated either by mathematical modelling, previous hands-on experience, or by actual measurement.

Target detections and target measurements are best observed in an environment, or theater, where they are not confused by the competing signatures or interferences of other objects.

Detection evaluations and tests are reasoned to be optimized where precise surface truth is available concerning the positions and movements of the participating objects and where the area is free and clear of other targets. When these conditions are met, the terms of (9) can be more easily evaluated for detection efficiency; also, valuable operating experience can be gained for applying better and more robust estimates for S/N.

To explore the feasibility and efficacity for the terms of (9) in the estimation of S/N, and under the conditions of a controlled experiment, we investigate the detectability of several metal objects in the theater of the eastern north Pacific.

From the archived data of a previous orbiting microwave receiving system, we observed several metal objects (targets) for which precise surface truth is available. The segment of the eastern north Pacific that is viewed by the orbiting receiving system is illustrated in Fig. B-1 where several metal objects are deployed to participate in the detection experiment, specifically, an aircraft and a ship.

The orbiting receiving system operates in an antenna scanning mode where the axis of the maximum gain, through the principal lobe of the directivity pattern G_{max}, is programmed to scan the width limits of the surface segment under surveillance. The scanning pattern consists of conterminous swaths that are executed by G_{max}. The swath time is 2 seconds. 48 signal intensity measurements are reported at intervals across each time tag with assigned geodetic coordinates that are dimensioned precisely in latitude and longitude.

The distance separating the swath traces for G_{max} is sufficiently small to allow some overlap of the antenna gain pattern to extend into the immediately adjacent swaths. This is a useful feature because the same observed target appears in adjacent swaths. From this, redundancy in the measurement occurs and the possibility of measuring a spurious signal is eliminated. The width of the scanned segment as projected on the Earth is 603 km.

The procedure for measuring S/N is the same for all objects.

The precise coincidence of time/lat/long for the metal object and for G_{max} is first established. Time/lat/long is determined for the object from its surface truth record. Typically, the precise time and the exact geodetic coordinates are determined by interpolation. Time/lat/long tags are assigned to each of the 48 swath intervals. When these data sets are brought into coincidence, the signature of the object is recorded.

For metal objects appearing as targets against a warm background, the receiver reports a colder temperature (low microwave flux level). Most orbiting receivers are, by choice, designed to show a decrease in the digital counts for cold targets.

The detailed flight schedule for the aircraft is given in Table B-1. The time interval for the surface truth record is taken from the on-board flight recorder for the expected time of the overflight.

The surface truth for the OSS Oceanographer is given in Table B-2.

The surface truth for the CV-990 and the OSS Oceanographer is given in Surface Truth Data Inventory, 15 February 1979, JPL Internal Document 622-99.

The data in Tables B-3 and B-4 deal only with the primitive digital counts given in the archived record.

For each metal object the standard error of estimate SEE of the T_B hyperplane is calculated in the immediate vicinity of the object. The SEE contains background temperature variations in T_B, clutter temperatures that enter the sidelobes and the backlobes, and receiver noise. From the SEE, the noise power P_i in (5) is calculated.

Table B-4 shows the details of measurements taken on metal objects during another experiment.

Calculated estimates for S/N from (9) and from the measured values given in Tables B-3 and B-4 are in satisfactory agreement. The degree of the agreement and the details that explain their differences are beyond the intended scope of this document.

The satellite sensor data records, and the surface truth that supports the measurements reported here, are abundantly available in the public domain. Investigators are invited to reconstruct the experiment and to compare results.

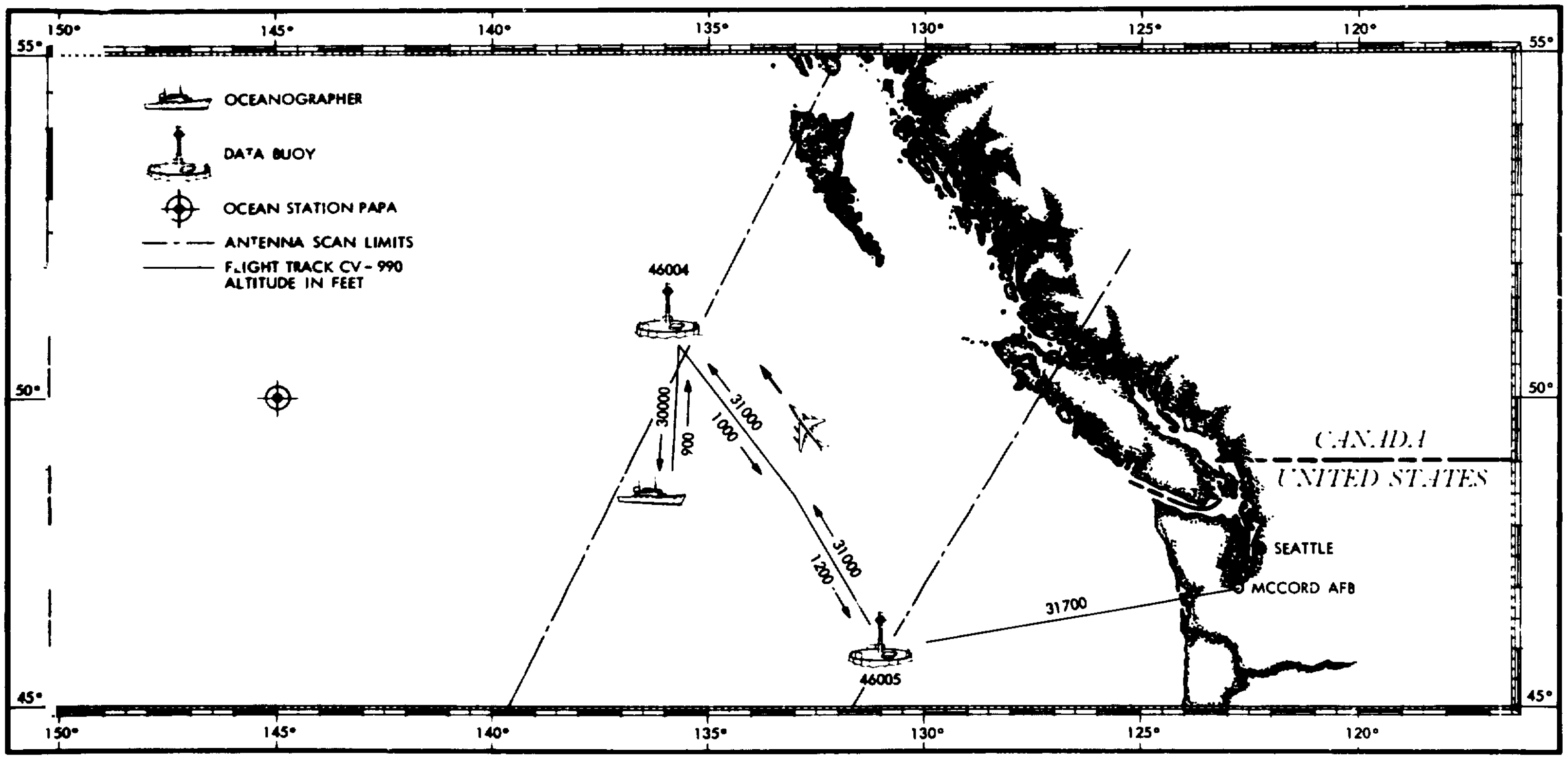

Fig. B-1. Flight of CV-990A on September 16, 1978 for orbit 1163, time 0533-0842 (GMT)

NASA CV-990A

NRL RP-3A

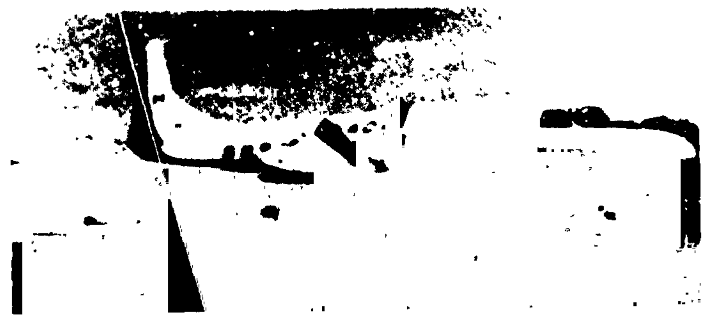

Canadian CV-580

Fig. B-2. Aircraft

Fig. B-3. Canadian Coast Guard Cutter Vancouver

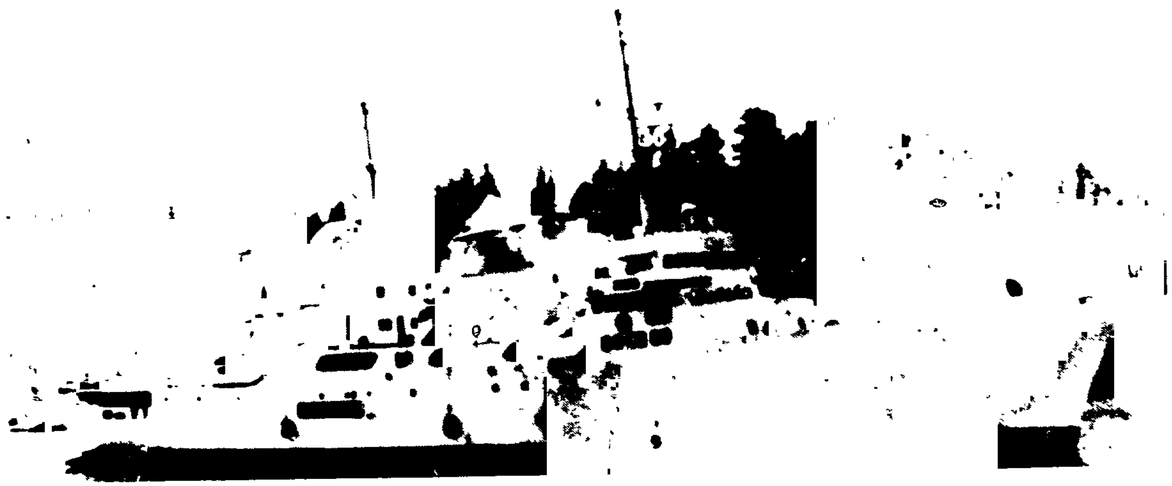

Fig. B-4. OSS Oceangrapher

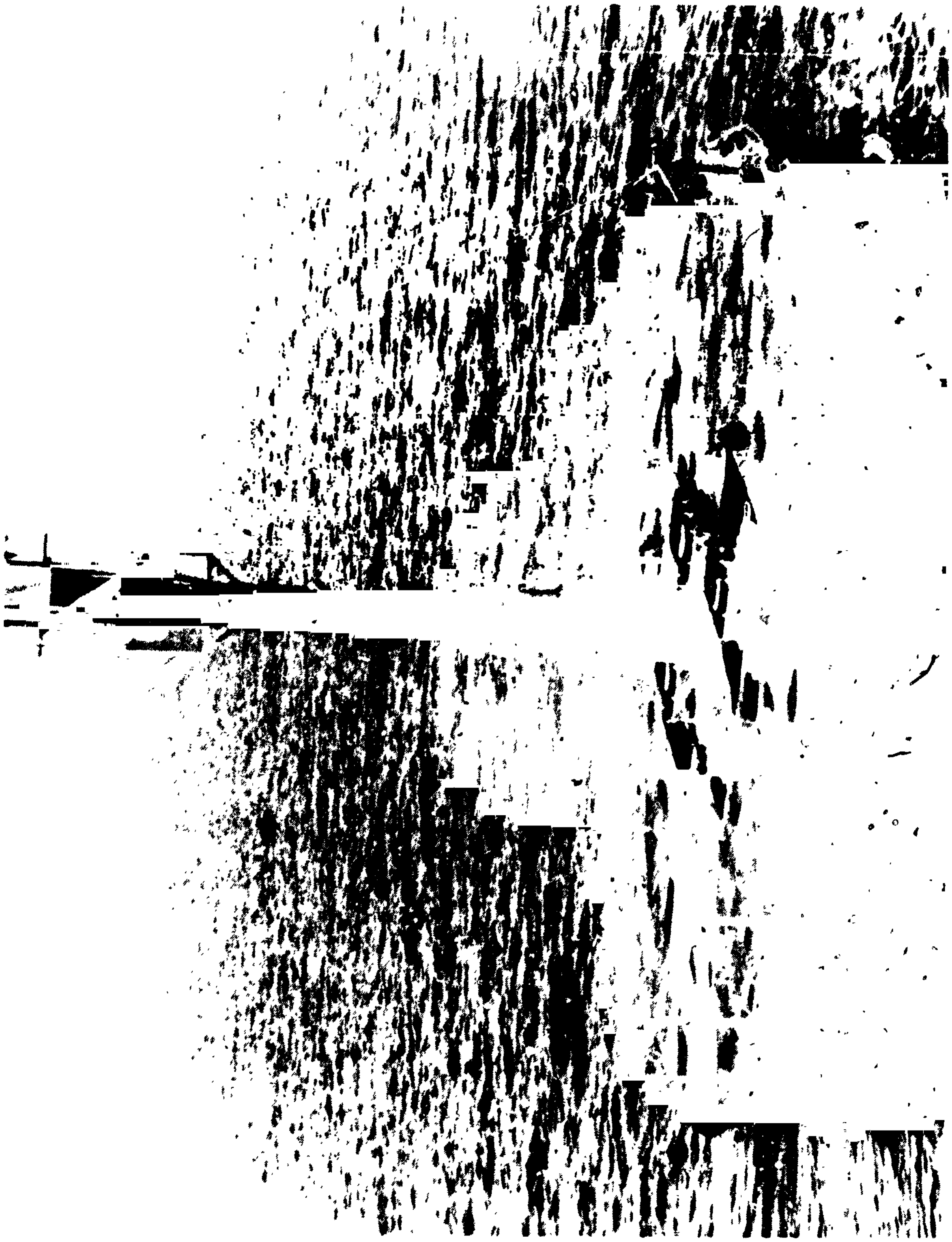

Fig. B-5. 12-meter Discus buoy

Fig. B-6. 6-meter Boat buoy (with corner reflectors)

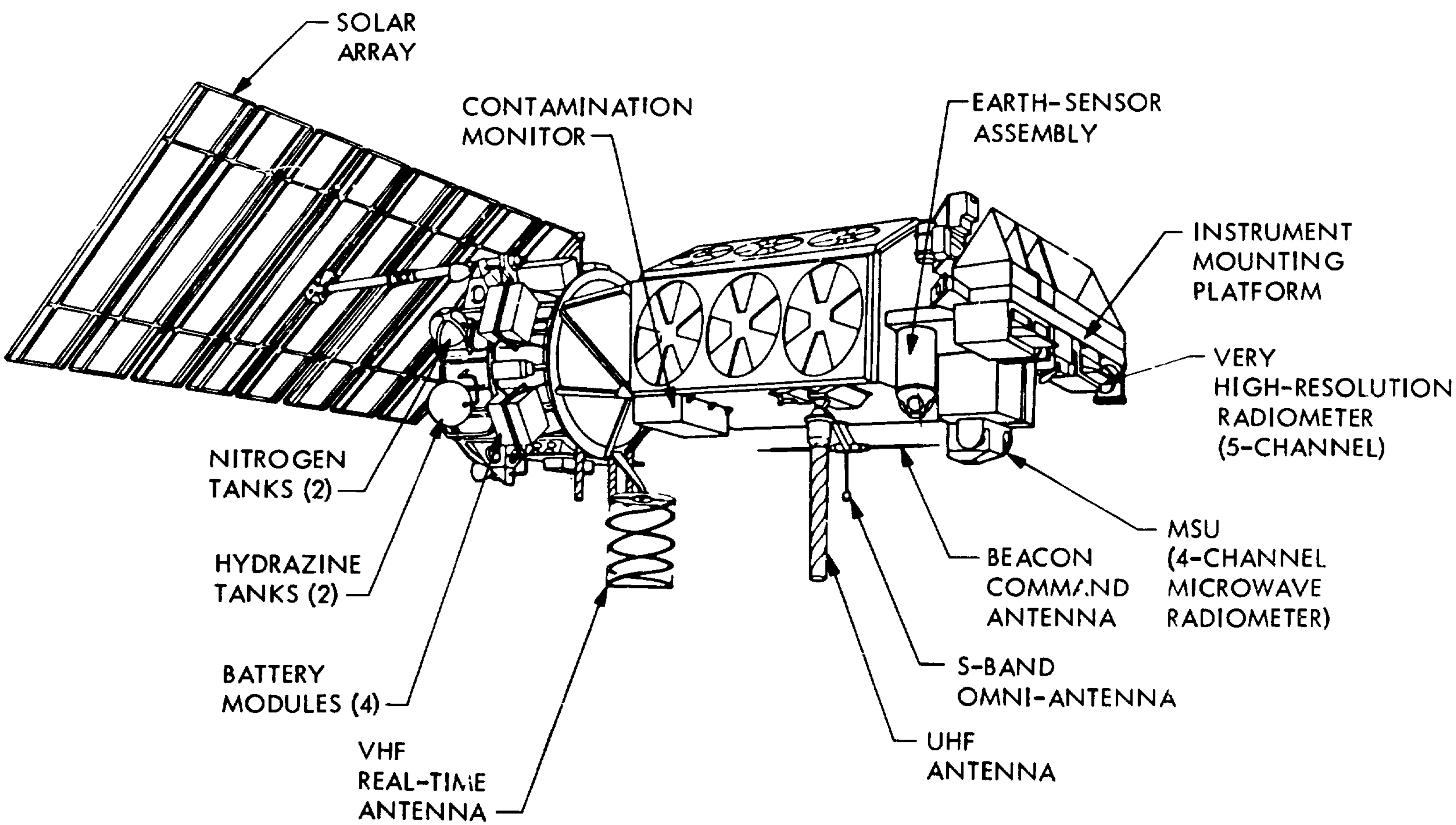

Fig. B-7. NOAA-C spacecraft

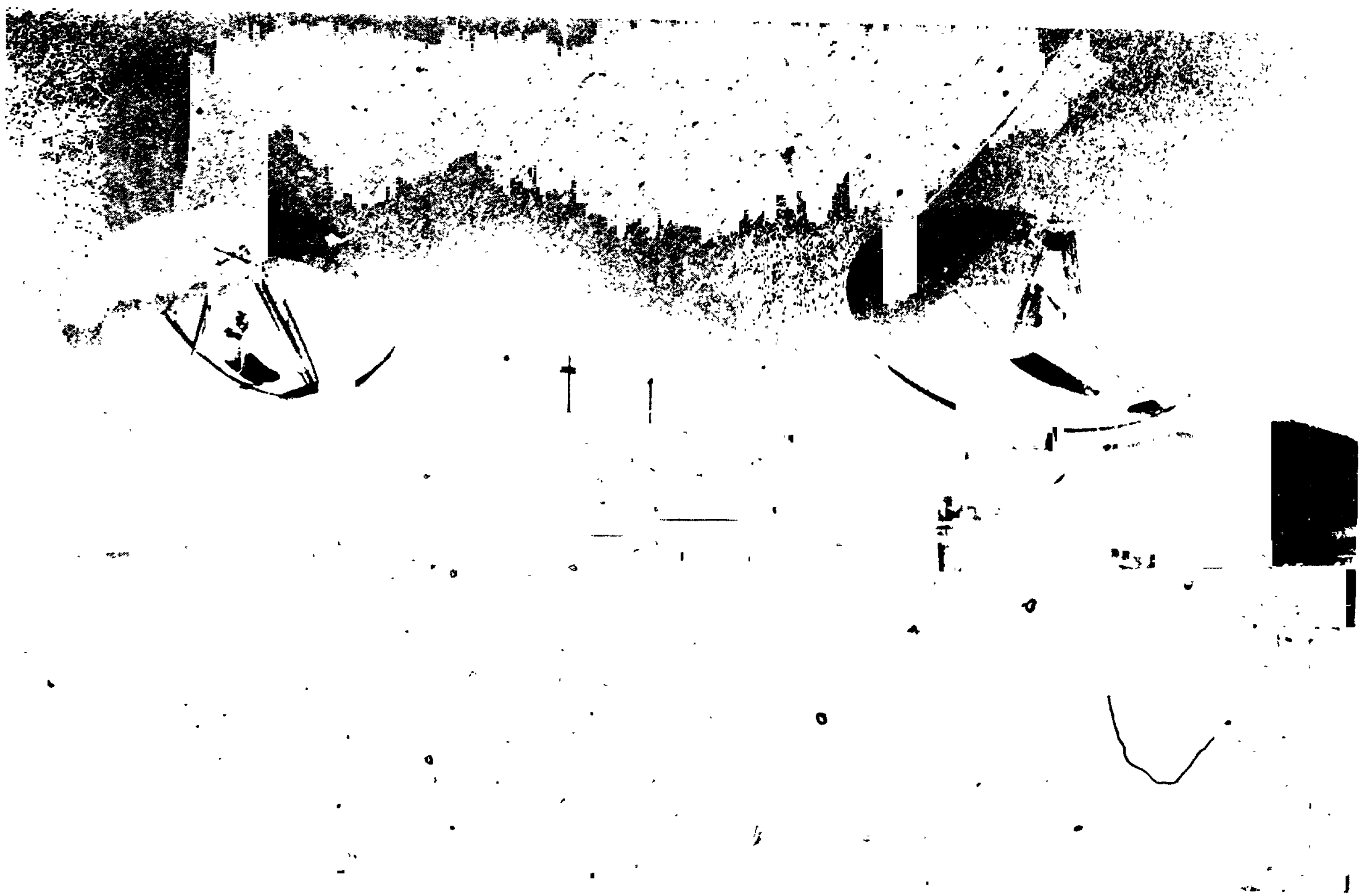

Fig. B-8. 64-meter antenna (right) near Canberra, Australia

ORIGINAL
OF POOR QUALITY

Fig. B-9. 64-meter antenna (left) near Madrid, Spain

Max-Planck-Institut für Radioastronomie Bonn

DAS RADIOTELESKOP IN EFFELSBERG

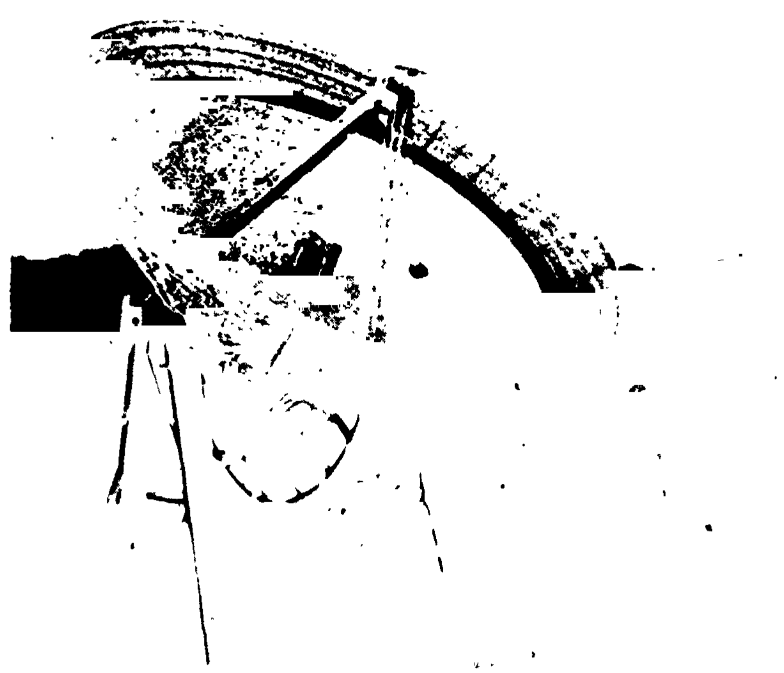

Fig. B-10. 100-meter antenna (Bonn, Germany)

OF POOR QUALITY

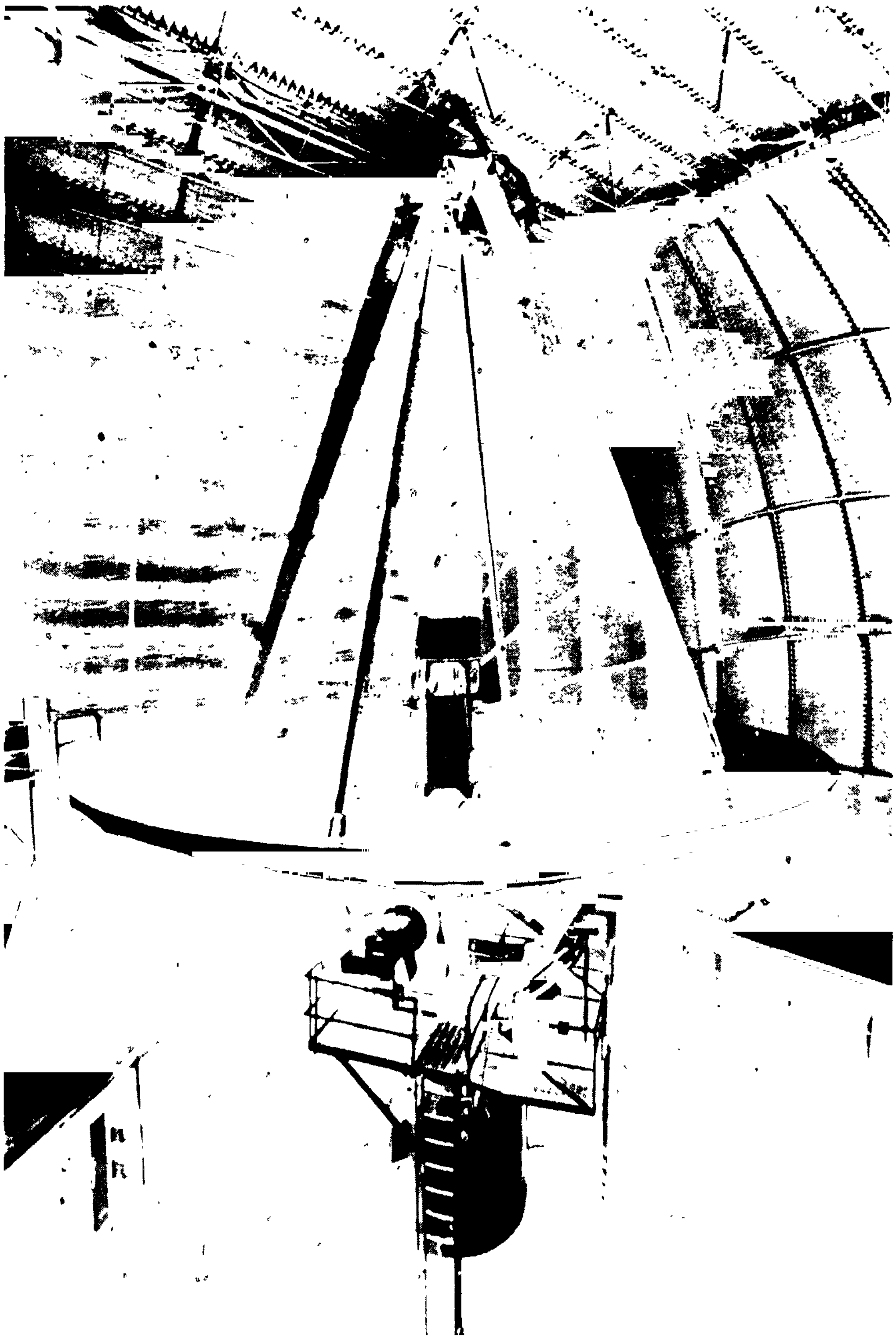

Fig. B-11. 10.79-meter antenna (Kitt Peak, Arizona)

ORIGINAL PAGE IS
OF POOR QUALITY

Fig. B-12. DSN, 64-meter antenna at Goldstone Dry Lake, California

Table B-1. Detailed flight schedule, spacecraft overflight times CV-990, September 16, 1978

TIME (Z)	LATITUDE (N)	LONGITUDE (W)	GROUND SPEED, kt	HEADING, deg	ALTITUDE, x 1000 ft
05:33:21	46° 04.5'	131° 02.8'	387	315	31.7
06:02:17	48° 43.0'	133° 18.5'	380	310	31.0
06:27:09	50° 51.7'	135° 49.8'	389	287	31.0
06:45:39	48° 36.8'	136° 00.0'	445	192	30.0
07:23:41	50° 51.9'	135° 58.9'	286	005	0.9
07:26:59	50° 47.6'	135° 44.5'	305	147	0.9
07:57:17	48° 43.1'	133° 18.3'	297	148	1.0
08:29:19	46° 30.5'	131° 41.3'	264	284	1.2
08:34:15	46° 22.1'	131° 17.9'	290	153	1.1
08:41:49	46° 00.7'	130° 59.0'	366	098	8.9

Table B-2. OSS Oceanographer (NOAA-101) positions, spacecraft overflight times

DATE	ORBIT	OVERFLIGHT TIME (Z)	LATITUDE	LONGITUDE
10 sept	1077	0748	48° 41.9'N	136° 19.4'W
	1083	1730	48° 40.9'N	133° 17.0'W
11 sept	1092	0858	48° 40.3'N	136° 57.4'W
12 sept	1106	0830	48° 40.0'N	141° 48.1'W
	1112	1816	48° 42.5'N	141° 39.5'W
13 sept	1120	0800	48° 41.9'N	136° 33.3'W
	1126	1742	48° 41.9'N	133° 17.7'W
14 sept	1135	0911	49° 42.4'N	136° 38.4'W
	1140	1714	48° 41.6'N	137° 59.6'W
15 sept	1149	0842	48° 41.3'N	140° 15.8'W
	1155	1824	48° 00.5'N	141° 05.7'W
16 sept	1163	0813	48° 27.1'N	136° 0.12'W
	1169	1755	48° 41.6'N	133° 17.8'W
17 sept	1183	1724	48° 42.2'N	133° 17.4'W
18 sept	1192	0855	48° 43.2'N	138° 42.8'W
	1198	1837	48° 42.2'N	141° 41.5'W
19 sept	1206	0826	48° 41.7'N	136° 24.4'W
	1212	1808	48° 42.1'N	133° 18.3'W
20 sept	1221	0936	48° 42.0'N	137° 10.5'W
	1226	1740	48° 41.8'N	138° 52.9'W

Table B-3. Observed objects from earth orbit (measured parameters - north Pacific area)

OBJECT	DATE AND TIME OF OBSERVATION yy/mm/dd/hh/mm/ss, Z	COORDINATES OF OBJECT LAT/LONG (SURFACE TRUTH) LAT/LONG (OBSERVED) DISTANCE IN km	ALTITUDE km	COURSE DEGREES TRUE	MEAN DIGITAL COUNTS NEAR OBJECT	SIGNAL DEVIATION FROM MEAN, COUNTS	SEE T_B HYPER-PLANE, COUNTS	S/N	S/N (dB)
CV-990 (NASA)	78/09/16/08/14/29	47.53N/132.44W 47.65N/132.34W 15	0.333	291	2402	-37.96	2.87	13.29	11.21
OSS-OCEANOGRAPHER (NOAA)	78/09/16/08/14/16	48.45N/136.00W 48.59N/135.85W 19	—	093	2380	-30.0	2.04	14.71	11.67
MERCHANT SHIP (CGBS)	78/09/16/08/14/04	*49.17N/133.2W 48.95N/133.85W 53	—	134	2375	-20.75	1.53	13.56	11.32

* POSITION ESTIMATED FROM 3 COORDINATES GIVEN OVER AN 18-HOUR PERIOD OF TIME

Table B-4. Measured parameters of objects observed from earth orbit (north Pacific area)

OBJECT	DATE AND TIME OF OBSERVATION yy/mm/dd/hh/mm/ss, Z	COORDINATES OF OBJECT Lat/Long (Surface Truth) Lat/Long (Observed) Distance in km	COURSE Degrees True	Mean Background Counts near Object	Number of Counts Deviation from Mean Background Counts	Std. Err. Est. Background Counts (Clutter Magnitude)	S/N	S/N (dB)	COMMENTS
BUOY (DISCUS) 46004 (NOAA)	78/08/31/07/40/05	51.00N/136.00W ..98N/135.98W 2.6	---	2337.29	-18.29	2.32	7.88	8.97	OPERATING WAVELENGTH • 8 mm SLANT RANGE • 1122 km COLLECTING APERTURE • 0.44 m^2 ATMOSPHERIC ATTEN. • 0.35 dB
VANCOUVER Coast Guard Cutter (CANADA)	78/08/31/07/40/25	50.10N/144.95W 50.08N/144.96W 2.3	UNDERWAY WITH NO WAY ON	2394.47	-28.6	5.83	4.91	6.91	SAME
UNIDENTIFIED OBJECT NEAR STATION PAPA	78/08/31/07/40/25	50.09N/144.81W 16.8 km NE (054 TRUE) OF STATION PAPA	---	2410.23	-38.23	7.16	5.34	7.27	SAME
OSS OCEANOGRAPHER NOAA-101	78/08/31/07/40/41	49.65N/141.18W 49.65N/141.21W 2.16	UNDERWAY WITH NO WAY ON	2403.22	-15.22	3.531	3.74	5.73	SAME